Title

A Comparison of Photocatalytic Activities of Gold Nanoparticles Following Plasmonic and Interband Excitation and a Strategy for Harnessing Interband Hot Carriers for Solution Phase Photocatalysis.

Journal

ACS central science, 3(5)

ISSN

2374-7943

Authors

Zhao, Jie
Nguyen, Son C
Ye, Rong
et al.

Publication Date

2017-05-01

DOI

10.1021/acscentsci.7b00122

Peer reviewed

ACS central science

Research Article

http://pubs.acs.org/journal/acscii

A Comparison of Photocatalytic Activities of Gold Nanoparticles Following Plasmonic and Interband Excitation and a Strategy for Harnessing Interband Hot Carriers for Solution Phase Photocatalysis

Jie Zhao,[†,‡] Son C. Nguyen,[†,‡,§] Rong Ye,[†,‡,∥,⊥] Baihua Ye,[†,‡] Horst Weller,[§,#] Gábor A. Somorjai,[*,†,∥,⊥,¶] A. Paul Alivisatos,[*,†,⊥,¶,Ψ] and F. Dean Toste[*,†,∥]

[†]Department of Chemistry, University of California, Berkeley, California 94720, United States

[§]The Hamburg Centre for Ultrafast Imaging, Luruper Chaussee 149, 22761 Hamburg, Germany

[∥]Chemical Sciences Division, Lawrence Berkeley National Lab, Berkeley, California 94720, United States

[#]Institute of Physical Chemistry, University of Hamburg, Grindelallee 117, 20146 Hamburg, Germany

[Ψ]Department of Materials Science and Engineering, University of California, Berkeley, California 94720, United States

[⊥]Kavli Energy NanoScience Institute, University of California, Berkeley, and Lawrence Berkeley National Lab, Berkeley, California 94720, United States

[¶]Materials Sciences Division, Lawrence Berkeley National Laboratory, Berkeley, California 94720, United States

Supporting Information

ABSTRACT: Light driven excitation of gold nanoparticles (GNPs) has emerged as a potential strategy to generate hot carriers for photocatalysis through excitation of localized surface plasmon resonance (LSPR). In contrast, carrier generation through excitation of interband transitions remains a less explored and underestimated pathway for photocatalytic activity. Photoinduced oxidative etching of GNPs with $FeCl_3$ was investigated as a model reaction in order to elucidate the effects of both types of transitions. The quantitative results show that interband transitions more efficiently generate hot carriers and that those carriers exhibit higher reactivity as compared to those generated solely by LSPR. Further, leveraging the strong π-acidic character of the resulting photogenerated Au^+ hole, an interband transition induced cyclization reaction of alkynylphenols was developed. Notably, alkyne coordination to the Au^+ hole intercepts the classic oxidation event and leads to the formation of the catalytically active gold clusters on subnanometer scale.

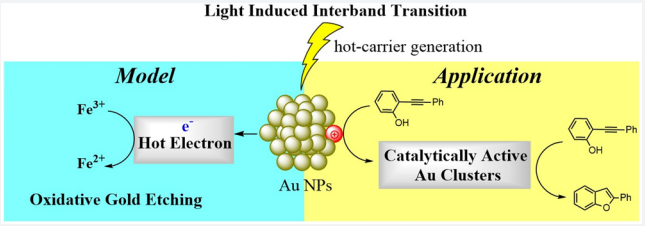

INTRODUCTION

Plasmonic noble metal nanoparticles (such as those of Au, Ag, or Cu) exhibit strong light absorption through excitation of a localized surface plasmon resonance (LSPR). The strong light absorption, robust nature, recyclability, and large surface areas of these nanoparticles render them candidates as photocatalytic materials. Therefore, these nanoparticles have recently been examined as photocatalysts for selective chemical synthesis by harvesting visible light to drive reactions at ambient conditions.[1,2] Although the catalytic mechanism is not fully understood, hot carriers (here referred to as high kinetic energy carriers) generated from surface plasmon excitation have been strongly implicated for driving some catalytic reactions.[1,3,4] These plasmonic noble metal nanoparticles also have strong absorption on the high-energy side of their plasmon resonances due to intrinsic interband transitions (Figures 1B and 2A). Limited studies of gold nanoparticles supported on metal oxides show higher photocatalytic activities in oxidation reactions for interband transitions as compared to that of LSPR. The higher potential for the interband transition results from the creation of a hot hole with a high reduction potential in the d band and a hot electron, to some extent, in the sp band.[5−7]

To gain insights into how hot carriers are generated under specific excitation wavelength, recent theoretical work predicted that photoexcitation of Au or Ag nanoparticles with photon energy below the interband energy can create hot s electrons or hot s holes in the intraband. However, when the photon energy is above the interband energy threshold, more hot carriers are generated from direct excitation of d−sp transitions even though these carriers do not have as high kinetic energy as those produced in the intraband transition.[8] These findings imply that photoexcitation at surface plasmon resonance, which usually has lower energy than the interband transition, does not produce hot carriers efficiently. This is not surprising when considering how the energy of an absorbed photon is divided in these two excitation regimes. In a classical description (Figure 1A, left), the LSPR photon energy is split between carriers in the sp band and their distribution among all continuous energy

Received: March 18, 2017
Published: May 15, 2017

DOI: 10.1021/acscentsci.7b00122
ACS Cent. Sci. 2017, 3, 482−488

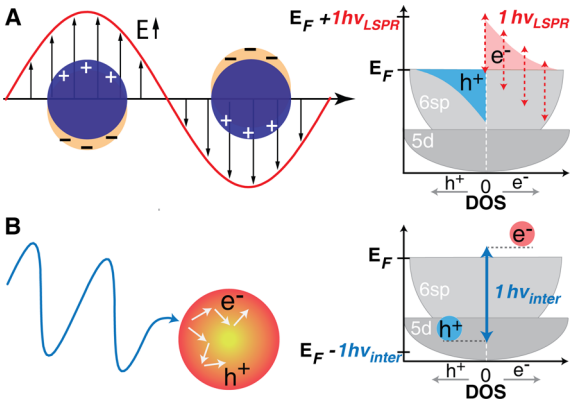

Figure 1. Carriers generated after photoexciting metallic nanoparticles at the LSPR and interband transition. (A) A classical description of LSPR shows oscillation of collective electrons driven by the electric field (left). The LSPR decay generates a population of hot carriers at various energies (right). The integral energy of both e^- (red area) and h^+ (blue) occupation is equivalent to a single photon energy. A quantum mechanical description of LSPR uses red arrows to represent a superposition of multiple isoenergetic, single-electron transitions when one photon is absorbed. (B) Interband transition results from absorption of a higher energy photon (left) and directly generates an e^-–h^+ pair (right).

states approximately follows a Fermi–Dirac distribution after the LSPR decays.[1] Consequently, the probability of having high-energy carriers is very low (Figure 1A, right). A more rigorous description is a quantum mechanical picture of superposition of many single-electron, quantized energy transitions (Figure 1A, right).[4] When considering momentum conservation in this discrete energy picture, the hot carrier generation is relatively weak because there is only a limited joint density of states in the particles with finite momentum that are matched with the LSPR wave vector.[8] In contrast, interband transitions efficiently create hot carriers because the photon energy is concentrated to a hot electron–hole pair (Figure 1B, right). In this regard, an important question is raised: is the ability to generate low populations of higher kinetic energy carriers (i.e., hotter carriers) by LSPR responsible for the observed light-driven catalysis by plasmonic metal nanoparticles, as compared to interband transitions, which produce a larger number of "cooler" hot carriers? In this work, we provide evidence to support the latter mechanism.

RESULTS AND DISCUSSION

Photoinduced Etching of Gold Nanorods. Recent research on photocatalysis of plasmonic nanoparticles has shifted heavily toward elucidating catalytic activity originating from LSPR and away from catalysis induced by interband transitions. In contrast, there is a dearth of experimental assessment of these two excitation pathways and the resulting mechanism of catalysis. Herein, the photocatalytic activities of gold nanoparticles following LSPR and interband excitation are compared in two reactions: the oxidative etching of gold nanoparticles with $FeCl_3$ and the cyclization of 2-(phenylethynyl)phenol. Colloidal gold nanorods (GNRs) and spheres (GNSs) were chosen as photocatalysts to avoid any effect from supporting or heterojunction materials. Moreover, GNRs have longitudinal LSPR absorption that is well separated from the interband transition absorption, allowing the evaluation of only the contribution of LSPR to the photocatalysis. Comparison of the catalytic performance of the particles as a function of the excitation wavelength supports the conclusion that interband transitions provide for greater catalytic activity than direct LSPR.

In the first reaction, the etching rates of GNRs and GNSs by a $FeCl_3$ solution in the dark and LSPR and interband excitations were compared. GNRs and GNSs gave similar results in this reaction; therefore GNRs were selected for examination. Previous studies have shown that, under dark conditions, etching occurs selectively at the tips of the GNRs and follows eq 1 because the gold ion product creates a strongly coordinated complex with halide ions so that the reduction potential of Au^+/Au is lower than that of Au^{3+}/Au and Fe^{3+}/Fe^{2+}.[9] To quantify the reaction rate, the blue-shifting rate of the longitudinal LSPR absorption was measured (Figure S2). This absorption peak is an effective probe for reaction rate as it is well separated from absorption of other reactants and products in solution. TEM and UV–vis spectroscopy proved a

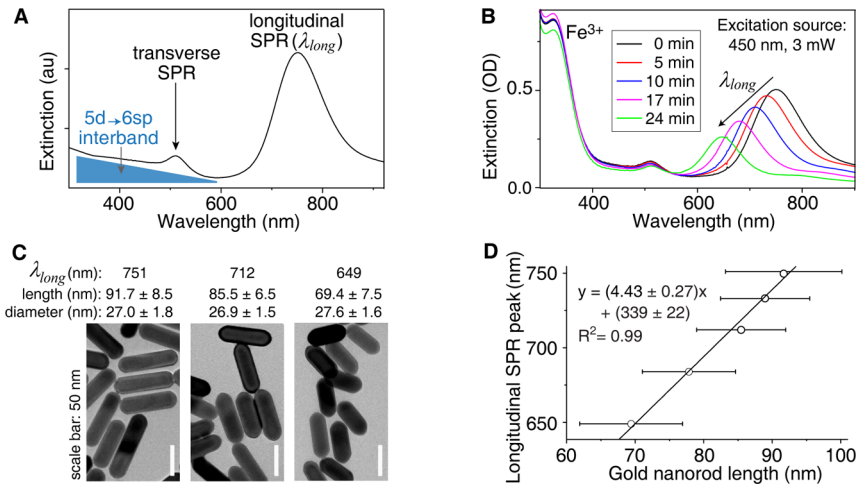

Figure 2. Photoinduced fast etching of GNRs in an $FeCl_3$ solution at room temperature. (A) Optical spectra of colloidal CTAB capped GNRs in water with depiction of the interband and LSPR absorptions. (B) Spectral progression of a typical reaction under 450 nm excitation. (C) Representative TEM images and average particle sizes showing tip etching of GNRs in B. (D) Linear dependence of λ_{long} vs GNR length (data in Table S3). The fitting does not propagate the errors in length to the final errors of intercept and slope values.

DOI: 10.1021/acscentsci.7b00122
ACS Cent. Sci. 2017, 3, 482–488

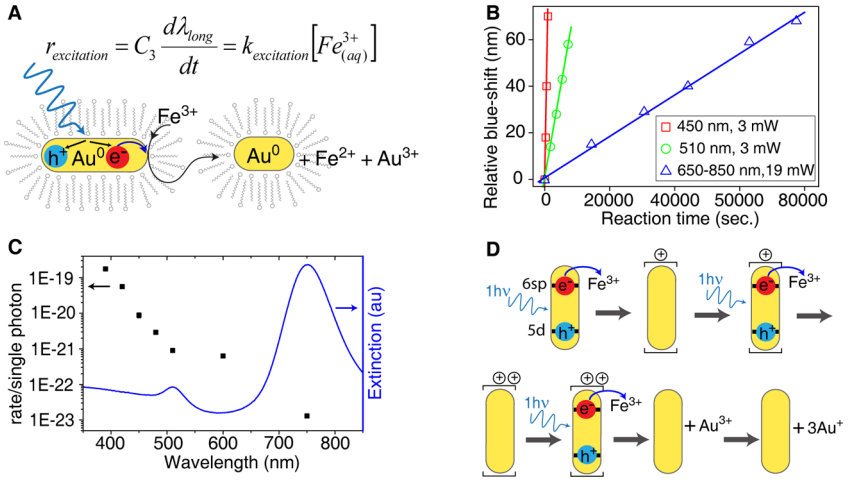

Figure 3. Kinetic studies of photoinduced fast etching of GNRs in an $FeCl_3$ solution at room temperature. (A) Illustration of that photoexcitation promotes fast etching, and the reaction rate is measured via the blue-shifting rate of the longitudinal SPR absorption (Supporting Information). (B) The etching rates at various wavelengths and absorbed photon powers. (C) Reaction rate normalized to each single photon absorbed, with respect to optical spectra of GNRs. (D) Proposed mechanism of the etching reaction.

proportional dependence of this blue-shifting rate to reaction rate due to the selective etching at the GNR tips (see the Supporting Information). A first order rate constant of k_{dark} = 3.41×10^{-7} s^{-1} was measured. The reaction showed first order dependence on $[Fe^{3+}]$ and an activation energy of 2.87 kcal/mol. These observations are consistent with homogeneous reaction with low absorption of Fe^{3+} on the GNR surface.

$$Fe^{3+}_{(aq)} + Au_{(s)} \rightarrow Fe^{2+}_{(aq)} + Au^{+}_{(aq)} \quad (1)$$

In order to study the light driven reaction, a monochromatic light source from a xenon lamp equipped with narrow band-pass filter (10−12 nm fwhm) was used and the reaction was monitored via a UV−vis spectrometer after various irradiation times (Figure 2B). TEM inspection showed a similar tip etching profile as in the reaction performed in the dark (Figure 2C). Upon photoexcitation, the etching reaction occurred through a pathway that generates soluble Au^{3+} as an intermediate that further etches the GNRs (see eqs S8 and S9 in the Supporting Information). However, the overall reaction still followed eq 1. The reaction rate was again measured via the blue-shifting rate of the longitudinal LSPR absorption (Figures 2D, 3A, 3B). At first glance, the etching rate appears faster under photoexcitation. Noticeably, interband excitation resulted in the highest etching rate while the rate following longitudinal LSPR excitation showed only an incremental difference as compared to k_{dark} (Table S1). Kinetics studies confirmed the first order of $[Fe^{3+}]$ in the rate equation and the linear dependence of the reaction rate to the excitation power (Supporting Information). Moreover, the increase in local temperature around the GNRs is very small (<1 K), and the rise in temperature of the reaction solution is just a few degrees above room temperature (Table S1) under our experimental conditions, and therefore the photothermal enhancement of the reaction rate can be ignored.[10,11] Taken together, these observations support the hypothesis that photoexcitation is responsible for promoting the etching reaction. It is important to note that the self-catalysis and the simplicity of this reaction provide a good model to understand the catalysis of hot carriers.

Since the reaction rate constant increased linearly with the photon flux, the rate constant, $k_{excitation}$, was normalized per single photon absorbed so that the rate can be compared properly across excitation wavelengths (Figure 3C, section I.1 in the Supporting Information describes how to quantify the absorbed but not the scattered photons). Strikingly, the rate constant was 3 to 4 orders of magnitude higher for the interband transition as compared to the longitudinal LSPR. The rate in the region of 480 to 600 nm excitation did not show a catalytic enhancement due to the transverse LSPR. In fact, the rate in this region was still very high as compared to the longitudinal LSPR due to the tail of the interband absorption starting at ~600 nm.[12] The quantum yield also exhibited a similar trend (Figure S10A). As mentioned in the previous paragraph, the high energy photon does not provide enough thermal energy to activate the reaction, regardless of the photon energy; therefore the increase of the reaction rate is mainly due to the higher efficiency of generating carriers. Finally, in order to probe the perspective of observing this reaction under sunlight, we simulated the reaction rates at each wavelength after accounting for the solar spectrum and the GNR optical absorption (Figure S10B). The calculated rates remained a few orders of magnitude higher activity for the interband excitation.

A stepwise mechanism for the etching reaction is proposed (Figure 3D). The first absorbed photon promotes an interband transition that results in a hot electron that reduces Fe^{3+} on the surface of the GNR to give an Fe^{2+} product and effectively leaves a positive charge on the GNRs. This step is repeated three times to produces an Au^{3+} product. The Au^{3+} further reacts with the GNRs to give the final product Au^{+}. This mechanism is supported by our detection of Au^{3+} intermediates, the observation of Au^{3+} further etched GNRs immediately after stopping irradiation, and that hole scavengers (acetone, methanol) resulted in decreased reaction rates (Supporting Information). With this mechanism of hot carriers catalyzing the reaction, the aforementioned reaction rates and quantum yield measurements indicate a significantly better efficiency of generating hot carriers for catalysis via interband transition as compared to direct surface plasmon excitation. These observations and conclusions beg the next question: can this mechanism be harnessed effectively for catalysis in liquid solution?

DOI: 10.1021/acscentsci.7b00122
ACS Cent. Sci. 2017, 3, 482−488

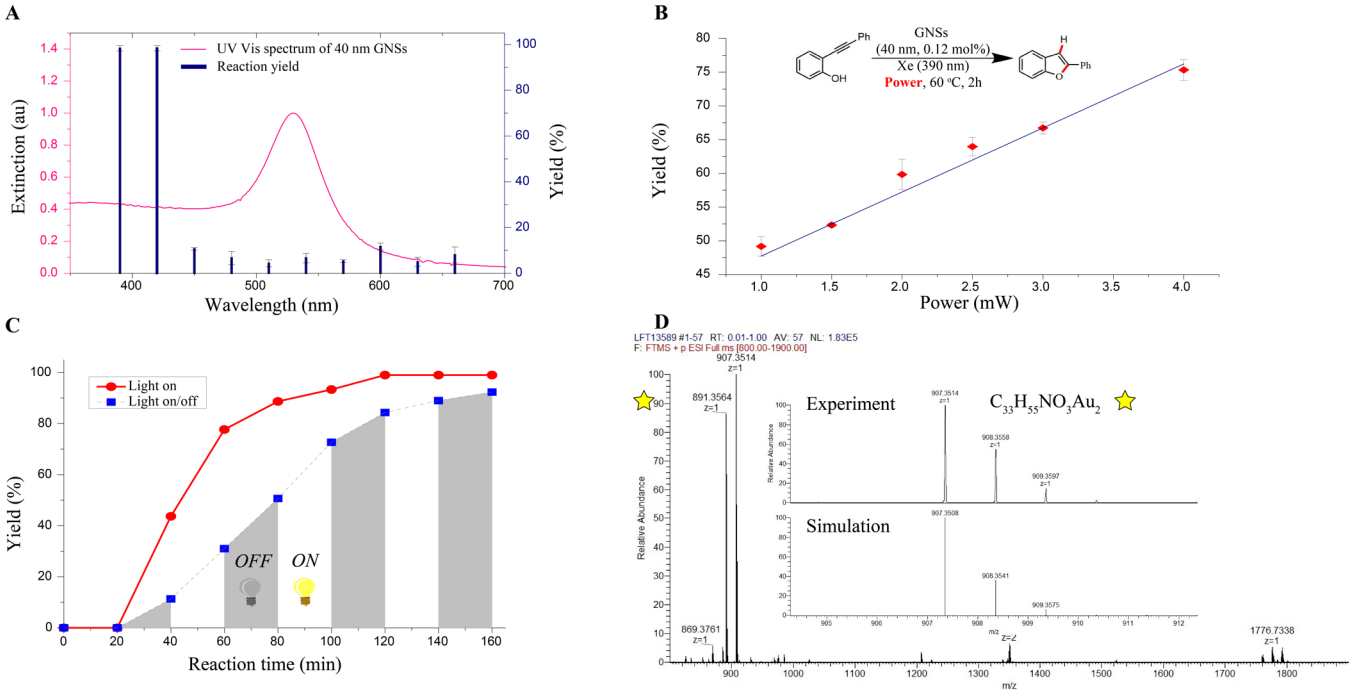

Figure 4. Photoinduced gold nanoparticle catalysis. (A) UV−vis spectrum of GNSs (diameter = 40 nm) and the catalytic activities of aforementioned GNSs using light source at various wavelength. Number of incident photons was normalized. (B) The power dependence of reaction yield using GNSs as catalyst and xenon lamp with 390 nm filter. (C) Plot-time−conversion studies under both "light always on" (red) and "light on/off" (blue) conditions; gray shadow means during this period the light was turned off and reaction was under dark conditions. 23W CFL was used as light source. (D) The major Au_2 cluster formed in situ in supernatant and detected by HR-ESI mass spectroscopy. See HR-ESI assignment of other Au_2 and Au_4 clusters in the Supporting Information.

Photoinduced Gold Nanoparticle Catalysis. Over the past decades, several studies involving light driven oxidation[13−20] and reduction[21−28] reactions catalyzed by semiconductor supported gold nanoparticles (GNPs) excited at their plasmon resonance have been described.[29] In these studies, a semiconductor support is often required to perform the electron−hole separation. Notably, the probability of interband transition, based on the intensity of optical absorption, accounts for roughly 50% of the overall optical absorption at the transverse LSPR frequency of GNRs or at the single LSPR frequency of GNSs. Therefore, we hypothesized that photocatalysis activities observed at the plasmon frequency in some of these studies might originate from the hidden tail of the interband transition similar to those observed in the etching study described above.

Photoinduced nanoparticle-catalyzed redox reactions are proposed to occur by a mechanism involving transfer of a hot electron on the surface of the semiconductor bulk, resulting in formation of a hole at the metal. In accord with this classic operational mode and the mechanism proposed above for carrier generation in GNPs via interband transition, we envisioned improved generation of hot carriers for catalysis. More specifically, we posited that the photogenerated Au^+ hole would have strong π-acidic character,[30−33] which could be leveraged for alkyne activation to intercept the oxidation event and drive to downstream catalysis.

On the basis of this hypothesis, 2-(phenylethynyl)phenol was chosen as a model substrate, and the corresponding cyclization reaction has been previously studied using gold nanoparticle catalysts and chemical oxidants.[34] CTAB-coated gold nanospheres with 40 nm diameter were initially used as catalysts in the cyclization. Additional CTAB was necessary for stabilizing the catalyst and solublizing the alkynylphenol into the aqueous media. The GNS-catalyzed reaction at 60 °C under 26 W household fluorescent compact light (CFL) irradiation produced 2-phenylbenzofuran in excellent yield (99%). On the other hand, blank and dark experiments in the absence of the catalyst and light irradiation respectively gave only trace amounts of the benzofuran product (<5%). Given these observations, the influence of incident light on the performance of cyclization was studied using xenon light with various wavelengths ranging from 390 to 660 nm with normalized incident photon numbers (Figure 4A). The studies found that the reaction proceeded with poor chemical conversions under the irradiation of light with wavelengths ranging from 480 to 660 nm. Notably, the low conversion at LSPR suggests that the cyclization was not driven effectively by the local surface plasmonic effect. On the other hand, nearly quantitative yields of the desired benzofuran were obtained when irradiating the reaction mixture in the near-ultraviolet region (390 and 420 nm). The same trend in reaction conversions was obtained when using GNSs with various diameters as well as GNRs with different aspect ratios (see the Supporting Information). In addition, a nearly linear relationship between the conversion of phenol and the power of the incident light was established (Figure 4B). These results advocate for a mechanism wherein hot carriers from interband excitation have a dramatic impact on the performance of cyclization. We noted that the reaction conversion showed drastic change when moving to near-ultraviolet excitation and that this trend does not correlate proportionally to the interband absorption as in Figure 2A. While a clear explanation for the phenomenon awaits further study, we posit that the reaction may have a threshold at a

DOI: 10.1021/acscentsci.7b00122
ACS Cent. Sci. 2017, 3, 482−488

particular photon energy for the formation of the catalytically active clusters.

In order to gain further insight into the mechanism of the photocatalysis, plot-time−conversion studies were performed under both "light always on" and "light on/off" conditions (Figure 4C). A reaction-induction period with "light on" of 20 min was observed, after which the product was steadily formed even without further light irradiation. Examination of the supernatant (see the Supporting Information) revealed that during the irradiation period a soluble catalyst was formed in situ from the GNPs. Most notably, several subnanosized Au_2 and Au_4 clusters complexed with the phenol substrates were identified in the supernatant solution by HR-ESI mass spectroscopy (Figure 4D). In accord with observations of Corma[35] and Hutchings,[36] these subnanosized clusters exhibit striking reactivity as catalysts in the cyclization reaction. In terms of scope, alkynylphenols with steric or electronic modifications on both arenes were found to be compatible under the same reaction conditions, affording the corresponding benzofurans in good yields (see the Supporting Information).

By analogy to the iron-promoted etching of GNPs, a mechanism involving initial interaction of alkynylphenol on the GNPs' surface was proposed (Figure 5). This alkynylphenol

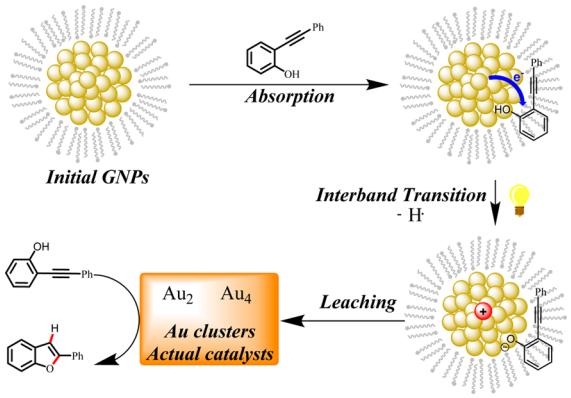

Figure 5. Proposed mechanism of the leaching process of GNPs.

substrate acts as the electron acceptor (much like Fe^{3+}) for the hot electron produced from the light-driven interband transition. Subsequent oxidation on the Au^+ hole and strong alkyne coordination to gold generates the corresponding nanoclusters that are leached into the solution. Compared to our previous catalysis[34,37−43] in the use of dendrimer capped GNPs with iodonium oxidants, the model phenol substrate plays a key role of not only an oxidant of GNPs but also a stabilizing ligand in the forming cluster.

CONCLUSIONS

While localized surface plasmon resonance (LSPR) provides a powerful platform for nanoparticle catalysis, our studies suggest that in some cases interband transitions should be considered as an alternative mechanism of light-driven nanoparticle catalysis. The benefits already demonstrated by plasmonic nanostructures as catalysts provided the impetus for examining complementary activation modes based on the metal nanoparticle itself. Leveraging these transitions has the potential to provide a means to highly active catalysis modes that would otherwise be challenging to access. For example, only a few methods have been reported for the preparation of highly active metal catalysts on a subnanosized scale, thus limiting their exploitation and study in catalysis.[44] This work suggests a novel and facile strategy for the formation of highly active gold nanocluster catalysts by light illumination of the interband transitions in the presence of the appropriate substrate. Finally, these studies implicated interband transitions, rather than LSPR, as important for the specific reactions and catalysts under study and should be applied judiciously beyond that. Indeed, it is likely that the activation mode will depend on catalyst features (metal, size, support) and the reaction and, therefore, warrants careful evaluation.

ASSOCIATED CONTENT

Supporting Information

The Supporting Information is available free of charge on the ACS Publications website at DOI: 10.1021/acscentsci.7b00122.

Synthetic procedures, kinetic study, supernatant experiments, recycling experiments, power efficiency, and HR-ESI and NMR studies (PDF)

AUTHOR INFORMATION

Corresponding Authors

*E-mail: fdtoste@berkeley.edu.
*E-mail: somorjai@berkeley.edu.
*E-mail: paul.alivisatos@berkeley.edu.

ORCID

Son C. Nguyen: 0000-0001-7713-4195
Horst Weller: 0000-0003-2967-6955
Gábor A. Somorjai: 0000-0002-8478-2761
F. Dean Toste: 0000-0001-8018-2198

Author Contributions

‡J.Z., S.C.N., R.Y., and B.Y. contributed equally.

Notes

The authors declare no competing financial interest.

ACKNOWLEDGMENTS

The gold catalyst experiment was supported by the U.S. Department of Energy, Office of Science, Office of Basic Energy Sciences, Chemical Sciences, Geosciences and Biosciences Division, under Contract DEAC02-05CH11231 (G.A.S., F.D.T.). Optic and chemical supply for the gold etching experiment was supported by the U.S. Department of Energy, Office of Science, Office of Basic Energy Sciences, Materials Sciences and Engineering Division, under Contract No. DE-AC02-05-CH11231 within the Physical Chemistry of Inorganic Nanostructures Program KC3103 (S.C.N., A.P.A.). J.Z. is grateful for The Dow Chemical Company who funded the Core−shell project under Contract 20120984. S.C.N. thanks the excellence cluster "The Hamburg Centre for Ultrafast Imaging—Structure, Dynamics and Control of Matter at the Atomic Scale" of the Deutsche Forschungsgemeinschaft (S.C.N., H.W.) for his postdoctoral appointment. B.Y. is grateful to the Swiss National Science Foundation (SNSF) for a postdoctoral mobility fellowship (P2ELP2_158881). We thank Dr. Rita Nichiporuk in QB3Mass lab for MS analysis, Dr. David Barton, Dr. Pete Nickias, and Dr. Trevor Ewers from the Dow Chemical Company, and Dr. Zhiqiang Niu for helpful discussions.

DOI: 10.1021/acscentsci.7b00122
ACS Cent. Sci. 2017, 3, 482−488

REFERENCES

(1) Brongersma, M. L.; Halas, N. J.; Nordlander, P. Plasmon-induced hot carrier science and technology. *Nat. Nanotechnol.* **2015**, *10*, 25−34.
(2) Linic, S.; Aslam, U.; Boerigter, C.; Morabito, M. Photochemical transformations on plasmonic metal nanoparticles. *Nat. Mater.* **2015**, *14*, 567−576.
(3) Brus, L. Plasmon-driven chemical synthesis: Growing gold nanoprisms with light. *Nat. Mater.* **2016**, *15*, 824−825.
(4) Moskovits, M. The case for plasmon-derived hot carrier devices. *Nat. Nanotechnol.* **2015**, *10*, 6−8.
(5) Zhu, H.; Chen, X.; Zheng, Z.; Ke, X.; Jaatinen, E.; Zhao, J.; Guo, C.; Xie, T.; Wang, D. Mechanism of supported gold nanoparticles as photocatalysts under ultraviolet and visible light irradiation. *Chem. Commun.* **2009**, 7524−7526.
(6) Liu, L.; Li, P.; Adisak, B.; Ouyang, S.; Umezawa, N.; Ye, J.; Kodiyath, R.; Tanabe, T.; Ramesh, G. V.; Ueda, S.; Abe, H. Gold photosensitized $SrTiO_3$ for visible-light water oxidation induced by Au interband transitions. *J. Mater. Chem. A* **2014**, *2*, 9875−9882.
(7) Hou, W.; Hung, W. H.; Pavaskar, P.; Goeppert, A.; Aykol, M.; Cronin, S. B. Photocatalytic Conversion of CO2 to Hydrocarbon Fuels via Plasmon-Enhanced Absorption and Metallic Interband Transitions. *ACS Catal.* **2011**, *1*, 929−936.
(8) Bernardi, M.; Mustafa, J.; Neaton, J. B.; Louie, S. G. Theory and computation of hot carriers generated by surface plasmon polaritons in noble metals. *Nat. Commun.* **2015**, *6*, 7044.
(9) Zou, R.; Guo, X.; Yang, J.; Li, D.; Peng, F.; Zhang, L.; Wang, H.; Yu, H. Selective etching of gold nanorods by ferric chloride at room temperature. *CrystEngComm* **2009**, *11*, 2797−2803.
(10) Keblinski, P.; Cahill, D. G.; Bodapati, A.; Sullivan, C. R.; Taton, T. A. Limits of localized heating by electromagnetically excited nanoparticles. *J. Appl. Phys.* **2006**, *100*, 054305.
(11) Nguyen, S. C.; Zhang, Q.; Manthiram, K.; Ye, X.; Lomont, J. P.; Harris, C. B.; Weller, H.; Alivisatos, A. P. Study of heat transfer dynamics from gold nanorods to the environment via time-resolved infrared spectroscopy. *ACS Nano* **2016**, *10*, 2144−2151.
(12) Khurgin, J. B. How to deal with the loss in plasmonics and metamaterials. *Nat. Nanotechnol.* **2015**, *10*, 2−6.
(13) Wang, J.; Ando, R. A.; Camargo, P. H. C. Controlling the selectivity of the surface plasmon resonance mediated oxidation of *p*-aminothiophenol on Au nanoparticles by charge transfer from UV-excited TiO_2. *Angew. Chem., Int. Ed.* **2015**, *54*, 6909−6912.
(14) Wang, C.; Astruc, D. Nanogold plasmonic photocatalysis for organic synthesis and clean energy conversion. *Chem. Soc. Rev.* **2014**, *43*, 7188−7216.
(15) Wang, F.; Li, C.; Chen, H.; Jiang, R.; Sun, L.-D.; Li, Q.; Wang, J.; Yu, J. C.; Yan, C.-H. Plasmonic harvesting of light energy for Suzuki coupling reactions. *J. Am. Chem. Soc.* **2013**, *135*, 5588−5601.
(16) Tsukamoto, D.; Shiraishi, Y.; Sugano, Y.; Ichikawa, S.; Tanaka, S.; Hirai, T. Gold nanoparticles located at the interface of anatase/rutile TiO_2 particles as active plasmonic photocatalysts for aerobic oxidation. *J. Am. Chem. Soc.* **2012**, *134*, 6309−6315.
(17) Tanaka, A.; Hashimoto, K.; Kominami, H. Preparation of Au/CeO_2 exhibiting strong surface plasmon resonance effective for selective or chemoselective oxidation of alcohols to aldehydes or ketones in aqueous suspensions under irradiation by green light. *J. Am. Chem. Soc.* **2012**, *134*, 14526−14533.
(18) Zheng, Z.; Huang, B.; Qin, X.; Zhang, X.; Dai, Y.; Whangbo, M.-H. Facile in situ synthesis of visible-light plasmonic photocatalysts M@TiO_2 (M = Au, Pt, Ag) and evaluation of their photocatalytic oxidation of benzene to phenol. *J. Mater. Chem.* **2011**, *21*, 9079−9087.
(19) Kowalska, E.; Abe, R.; Ohtani, B. Visible light-induced photocatalytic reaction of gold-modified titanium(IV) oxide particles: action spectrum analysis. *Chem. Commun.* **2009**, 241−243.
(20) Chen, X.; Zhu, H.-Y.; Zhao, J.-C.; Zheng, Z.-F.; Gao, X.-P. Visible-light-driven oxidation of organic contaminants in air with gold nanoparticle catalysts on oxide supports. *Angew. Chem.* **2008**, *120*, 5433−5436.
(21) Yang, J.; Li, Y.; Zu, L.; Tong, L.; Liu, G.; Qin, Y.; Shi, D. Light-concentrating plasmonic Au superstructures with significantly visible-light-enhanced catalytic performance. *ACS Appl. Mater. Interfaces* **2015**, *7*, 8200−8208.
(22) Li, P.; Ma, B.; Yang, L.; Liu, J. Hybrid single nanoreactor for in situ SERS monitoring of plasmon-driven and small Au nanoparticles catalyzed reactions. *Chem. Commun.* **2015**, *51*, 11394−11397.
(23) Kang, L.; Han, X.; Chu, J.; Xiong, J.; He, X.; Wang, H.-L.; Xu, P. In Situ Surface-Enhanced Raman Spectroscopy Study of Plasmon-Driven Catalytic Reactions of 4-Nitrothiophenol under a Controlled Atmosphere. *ChemCatChem* **2015**, *7*, 1004−1010.
(24) Hajfathalian, M.; Gilroy, K. D.; Yaghoubzade, A.; Sundar, A.; Tan, T.; Hughes, R. A.; Neretina, S. Photocatalytic Enhancements to the Reduction of 4-Nitrophenol by Resonantly Excited Triangular Gold−Copper Nanostructures. *J. Phys. Chem. C* **2015**, *119*, 17308−17315.
(25) Ding, Q.; Chen, M.; Li, Y.; Sun, M. Effect of aqueous and ambient atmospheric environments on plasmon-driven selective reduction reactions. *Sci. Rep.* **2015**, *5*, 10269.
(26) Collado, L.; Reynal, A.; Coronado, J. M.; Serrano, D. P.; Durrant, J. R.; de la Peña O'Shea, V. A. Effect of Au surface plasmon nanoparticles on the selective CO_2 photoreduction to CH_4. *Appl. Catal., B* **2015**, *178*, 177−185.
(27) Fasciani, C.; Alejo, C. J. B.; Grenier, M.; Netto-Ferreira, J. C.; Scaiano, J. C. High-Temperature Organic Reactions at Room Temperature Using Plasmon Excitation: Decomposition of Dicumyl Peroxide. *Org. Lett.* **2011**, *13*, 204−207.
(28) Zhu, H.; Ke, X.; Yang, X.; Sarina, S.; Liu, H. Reduction of nitroaromatic compounds on supported gold nanoparticles by visible and ultraviolet light. *Angew. Chem., Int. Ed.* **2010**, *49*, 9657−9661.
(29) Mukherjee, S.; Libisch, F.; Large, N.; Neumann, O.; Brown, L. V.; Cheng, J.; Lassiter, J. B.; Carter, E. A.; Nordlander, P.; Halas, N. J. Hot electrons do the impossible: plasmon-induced dissociation of H_2 on Au. *Nano Lett.* **2013**, *13*, 240−247.
(30) Dorel, R.; Echavarren, A. M. Gold (I)-catalyzed activation of alkynes for the construction of molecular complexity. *Chem. Rev.* **2015**, *115*, 9028−9072.
(31) Wang, W.; Hammond, G. B.; Xu, B. Ligand effects and ligand design in homogeneous gold(I) catalysis. *J. Am. Chem. Soc.* **2012**, *134*, 5697−5705.
(32) Gorin, D. J.; Sherry, B. D.; Toste, F. D. Ligand effects in homogeneous Au catalysis. *Chem. Rev.* **2008**, *108*, 3351−3378.
(33) Gorin, D. J.; Toste, F. D. Relativistic effects in homogeneous gold catalysis. *Nature* **2007**, *446*, 395−403.
(34) Witham, C. A.; Huang, W.; Tsung, C.-K.; Kuhn, J. N.; Somorjai, G. A.; Toste, F. D. Converting homogeneous to heterogeneous in electrophilic catalysis using monodisperse metal nanoparticles. *Nat. Chem.* **2010**, *2*, 36−41.
(35) Oliver-Meseguer, J.; Cabrero-Antonino, J. R.; Domínguez, I.; Leyva-Pérez, A.; Corma, A. Small gold clusters formed in solution give reaction turnover numbers of 10^7 at room temperature. *Science* **2012**, *338*, 1452−1455.
(36) Herzing, A. A.; Kiely, C. J.; Carley, A. F.; Landon, P.; Hutchings, G. J. Identification of active gold nanoclusters on iron oxide supports for CO oxidation. *Science* **2008**, *321*, 1331−1335.
(37) Gross, E.; Shu, X.-Z.; Alayoglu, S.; Bechtel, H.; Martin, M. C.; Toste, F. D.; Somorjai, G. A. In situ IR and X-ray high spatial-resolution microspectroscopy measurements of multistep organic transformation in flow microreactor catalyzed by Au nanoclusters. *J. Am. Chem. Soc.* **2014**, *136*, 3624−3629.
(38) Gross, E.; Toste, F. D.; Somorjai, G. A. Polymer-encapsulated metallic nanoparticles as a bridge between homogeneous and heterogeneous catalysis. *Catal. Lett.* **2015**, *145*, 126−138.
(39) Gross, E.; Liu, J.-H.; Alayoglu, S.; Marcus, M. A.; Fakra, S. C.; Toste, F. D.; Somorjai, G. A. Asymmetric catalysis at the mesoscale: gold nanoclusters embedded in chiral self-assembled monolayer as heterogeneous catalyst for asymmetric reactions. *J. Am. Chem. Soc.* **2013**, *135*, 3881−3886.
(40) Gross, E.; Liu, J. H.-C.; Toste, F. D.; Somorjai, G. A. Control of selectivity in heterogeneous catalysis by tuning nanoparticle properties and reactor residence time. *Nat. Chem.* **2012**, *4*, 947−952.

DOI: 10.1021/acscentsci.7b00122
ACS Cent. Sci. 2017, 3, 482−488

(41) Li, Y.; Liu, J. H.-C.; Witham, C. A.; Huang, W.; Marcus, M. A.; Fakra, S. C.; Alayoglu, P.; Zhu, Z.; Thompson, C. M.; Arjun, A.; Lee, K.; Gross, E.; Toste, F. D.; Somorjai, G. A. A Pt-cluster-based heterogeneous catalyst for homogeneous catalytic reactions: X-ray absorption spectroscopy and reaction kinetic studies of their activity and stability against leaching. *J. Am. Chem. Soc.* **2011**, *133*, 13527−13533.
(42) Huang, W.; Liu, J. H.-C.; Alayoglu, P.; Li, Y.; Witham, C. A.; Tsung, C.-K.; Toste, F. D.; Somorjai, G. A. Highly active heterogeneous palladium nanoparticle catalysts for homogeneous electrophilic reactions in solution and the utilization of a continuous flow reactor. *J. Am. Chem. Soc.* **2010**, *132*, 16771−16773.
(43) Jin, R.; Zeng, C.; Zhou, M.; Chen, Y. Atomically precise colloidal metal nanoclusters and nanoparticles: Fundamentals and opportunities. *Chem. Rev.* **2016**, *116*, 10346−10413.
(44) Ye, R.; Yuan, B.; Zhao, J.; Ralston, W. T.; Wu, C.-Y.; Unel Barin, E.; Toste, F. D.; Somorjai, G. A. Metal nanoparticles catalyzed selective carbon-carbon bond activation in the liquid phase. *J. Am. Chem. Soc.* **2016**, *138*, 8533−8537.

DOI: 10.1021/acscentsci.7b00122
ACS Cent. Sci. 2017, 3, 482−488